JGR Space Physics

RESEARCH ARTICLE
10.1029/2019JA026476

Radar Studies of Height-Dependent Equatorial *F* region Vertical and Zonal Plasma Drifts

S. A. Shidler[1], F. S. Rodrigues[1], B. G. Fejer[2], and M. A. Milla[3]

[1]W. B. Hanson Center for Space Sciences, University of Texas at Dallas, Richardson, TX, USA, [2]Center for Atmospheric and Space Sciences, Utah State University, Logan, Utah, USA, [3]Radio Observatorio de Jicamarca, Instituto Geofísico del Perú, Lima, Peru

Key Points:
- Long-term measurements of both vertical and zonal plasma drifts made by the Jicamarca ISR have been analyzed for quiet time conditions
- Results show the average behavior of height profiles of the drifts for different seasons and distinct solar flux conditions
- The results can be used to aid the interpretation of satellite observations and numerical model results

Correspondence to:
S. A. Shidler,
sas141430@utdallas.edu

Citation:
Shidler, S. A., Rodrigues, F., Fejer, B. G., & Milla, M. (2019). Radar studies of height-dependent equatorial *F* region vertical and zonal plasma drifts. *Journal of Geophysical Research: Space Physics*, *124*. https://doi.org/10.1029/2019JA026476

Received 7 JAN 2019
Accepted 17 FEB 2019
Accepted article online 25 FEB 2019

Abstract We present the results of an analysis of long-term measurements of ionospheric *F* region **E** × **B** plasma drifts in the American/Peruvian sector. The analysis used observations made between 1986 and 2017 by the incoherent scatter radar of the Jicamarca Radio Observatory. Unlike previous studies, we analyzed both vertical and zonal components of the plasma drifts to derive the geomagnetically quiet time climatological variation of the drifts as a function of height and local time. We determine the average behavior of the height profiles of the drifts for different seasons and distinct solar flux conditions. Our results show good agreement with previous height-averaged climatological results of vertical and zonal plasma drifts, despite that they are obtained from different sets of measurements. More importantly, our results quantify average height variations in the drifts. The results show, for example, the solar flux control over the height variation of the vertical drifts. The results also show the weak dependence of the daytime zonal drift profiles on solar and seasonal variations. We quantify the effects of seasonal and solar flux variations on the morphology of the vertical shear in the zonal plasma drifts associated with the evening plasma vortex. Assuming interchangeability between local time and longitude, we tested the curl-free condition for the *F* region electric fields with very good results for all seasons and solar flux conditions. We envision the use of our results to aid numerical modeling of ionospheric electrodynamics and structuring and to assist with the interpretation of satellite observations of low-latitude plasma drifts.

1. Introduction

The behavior of the geomagnetically quiet time ionospheric equatorial **E** × **B** *F* region plasma drifts near the magnetic equator is a manifestation of a complex current system driven, mainly, by thermospheric winds but with nonnegligible contributions from gravity and gradients in plasma pressure (Eccles, 2004).

F region plasma drifts can also serve as tracers of the underlying thermospheric conditions and ion-neutral coupling at *E* and *F* region heights. For instance, at night, equatorial plasma drifts are expected to follow, to some extent, the behavior of zonal winds at main *F* region heights (e.g., Coley et al., 1994; Herrero et al., 1985). Additionally, direct measurements of winds at thermospheric heights are difficult to make and have been limited in number, making plasma drift observations even more important for thermospheric studies.

Plasma drifts also control the structuring of the plasma at low latitudes over a wide range of scale sizes, with implications to fundamental studies of ionospheric irregularities and space weather. Vertical plasma drifts contribute with the plasma fountain effect and help distribute the equatorial plasma to low latitudes creating the equatorial anomaly and the so-called F_3 layer (Balan & Bailey, 1995). Vertical plasma drifts near sunset are also recognized to play an important role in the development of equatorial spread *F* (ESF) plasma structures with scale sizes ranging from a few centimeters to several hundreds of kilometers (Hysell, 2000; Woodman, 2009). It is well recognized that the stability of the equatorial *F* region is heavily controlled by the magnitude of the vertical drifts near sunset associated with the prereversal enhancement (PRE) of the zonal electric field (e.g., Fejer et al., 1999; Huang & Hairston, 2015; Kil et al., 2009a).

More recently, it has been shown that the stability of the equatorial *F* region is also affected by the behavior of the zonal plasma drifts. A region of retrograde plasma motion with respect to the neutral winds near the bottomside *F* region can create favorable conditions for the growth of a collisional shear instability, which is thought to contribute to ESF development and morphology (Aveiro & Hysell, 2010; Hysell & Kudeki, 2004; Kudeki & Bhattacharyya, 1999; Kudeki et al., 2007).

Given the importance of F region drifts, various studies using ground- and spaced-based observations have been conducted (e.g., Fejer et al., 2008; Kil et al., 2009b; Rodrigues et al., 2015; Scherliess & Fejer, 1999). The average behavior of plasma drifts as a function of season, longitude, and solar flux conditions has been derived using measurements made by sensors on satellites (e.g., Fejer et al., 2008; Kil et al., 2009a; Stoneback et al., 2011). These measurements, in general, have been made at topside F region altitudes where most of the satellites orbit. Observations near the F region peak, however, have been possible with the incoherent scatter radar (ISR) of the Jicamarca Radio Observatory, located at the magnetic equator near Lima, Peru. Semiroutine Jicamarca ISR observations have been made since the late 1960s, and a number of studies have presented the results of these observations. In general, each study focused on either zonal drifts (e.g., Fejer et al., 1981, 2005) or vertical plasma drifts (e.g., Fejer et al., 1979; Scherliess & Fejer, 1999). These studies, nevertheless, summarized the behavior of the equatorial F region plasma motion under different geophysical conditions including those affected by disturbances of magnetospheric origin (Fejer & Scherliess, 1995).

The studies mentioned above offered important insights on the electrodynamics of the low-latitude ionosphere based on height-averaged observations. Case studies, however, showed that plasma drifts can change significantly with altitude throughout F region heights (Fejer et al., 1985; Pingree & Fejer, 1987). The height-average approach was taken, for the most part, due to the limited number of usable height profile observations at the time of those studies. However, significant improvements in the ISR observations at Jicamarca (Kudeki et al., 1999) and continued measurements throughout the years now allow us to investigate the behavior of the drifts throughout F region heights for all local times under different seasons and solar flux conditions.

Here we present the results of a study of both zonal and vertical plasma drifts measurements made by the Jicamarca ISR between 1986 and 2017. We focus, in particular, on deriving climatological height profiles of quiet time drifts for different seasons and solar flux conditions. This report is organized as follows: In section 2, we provide details about the observations used in this study. We also provide details on how we selected usable observations, and how we organized these observations to derive the average profiles. The results of our analysis are presented and discussed in section 3. We examine how our results compare with previous studies and discuss the height variations observed in the zonal and vertical drifts. We also examine the validity of the curl-free approximation for the electric fields around the PRE. A brief summary describing the main implications of our study is presented in section 4.

2. Observations and Analysis

The ISR of the Jicamarca Radio Observatory, near Lima Peru (11.95°S, 76.67°W; dip latitude ~1° dip angle) is capable of making semiroutine observations of the equatorial F region plasma drifts. Observations of the zonal and vertical components of the plasma drifts are possible by combining measurements of line-of-sight plasma drifts obtained using two antenna beams. One antenna beam is pointed a few degrees (~2.5°) off-zenith to the east of the radar site, while another beam is pointed a few degrees to the west (Kudeki et al., 1999; Woodman, 1972). The ISR technique provides measurements of the drifts as a function of height and local time. Uncertainties for the zonal and vertical components of the drifts are also available.

In this study, we analyzed 599 days of measurements made between 1986 and 2017 that are available through the Madrigal database (http://jro.igp.gob.pe/madrigal/). Typically, the observations have a height resolution of 15–20 km, and a temporal resolution of about 5 min. Here we focus on the 200- to 600-km height range, which is the region typically covered by the observations for the most conditions of local time, season, and solar flux.

We also focus on the behavior of the drifts during geomagnetically quiet conditions. To select quiet days, we use the planetary K (K_p) geomagnetic index. We only use measurements where the K_p index at the time of the measurement and the three previous 3-hr K_p indices are less than 3. We have also removed measurements occurring during both minor and major sudden stratospheric warming events, which occur primarily in January and February (e.g., Chau et al., 2009, 2012). We must point out that each day does not necessarily have 24 hr of uninterrupted data collection. Furthermore, it does not necessarily have an equal number of vertical and zonal drift measurements.

To eliminate low-quality measurements, we followed a three-step selection process. First, the vertical (zonal) drifts with uncertainties greater than 10 m/s (95 m/s) were removed from the data set. This relatively relaxed

Table 1
Summary of Plasma Drift Observations Used in This Study

Season and solar flux	Observation days	Average solar flux (SFU) Vertical drifts (zonal drifts)
Equinox HSF	113	150
Equinox LSF	108	80
Jun solstice HSF	80	130
Jun solstice LSF	80	80
Dec solstice HSF	117	150
Dec solstice LSF	101	80

Note. HSF = high solar flux; LSF = low solar flux; SFU = solar flux unit.

condition on maximum uncertainty for the zonal drifts had little impact on data below 450 km and was chosen to ensure that a significant number of measurements above this altitude were still available for most seasons and solar flux conditions.

Second, we use SNR values as a way to detect the contamination of incoherent scatter echoes by coherent scatter echoes caused by field-aligned irregularities. Measurements with SNR values greater than ~1.0 dB were associated with ESF and discarded. Finally, outlier measurements were eliminated using the 1.5*IQR (interquartile-range) rule for the drifts (e.g., Baron, 2013). The resulting medians for daytime uncertainties below 450 km are 1–2 m/s for the vertical drifts, and 15–30 m/s for the zonal drifts, respectively, however, with somewhat higher uncertainty medians above 450 km. The uncertainties are slightly larger during nighttime and at higher altitudes due to reduced electron densities and signal-to-noise ratio (SNR) values of the measured echoes. These steps were applied only to the measurements between 1996 and 2017, when SNR values are provided with the drift measurements.

Finally, the measurements are binned by season, solar cycle, local time, and height. To increase the statistical significance of the mean drifts, we use 1-hr wide bins with centers spaced 30 min apart. An exception to this procedure occurs during the period between 1700 and 2200 LT where we have used 30-min wide bins with centers spaced 15 min apart. This is to capture the rapidly changing vertical drifts associated with the evening PRE of the vertical drifts. Altitude measurements are grouped into 80-km-wide overlapping bins with centers spaced by 40 km. The 4-month seasonal bins include equinox (March, April, September, and October), June solstice (May, June, July, and August), and December solstice (January, February, November, and December). Finally, data are binned into low solar flux and high solar flux conditions. Cutoff values of solar flux were chosen so that the average low solar flux and high solar flux for each season was 80 and 150 solar flux unit (SFU), respectively. June solstice lacks measurements during high solar flux conditions and resulted in the high solar flux average to be 130 SFU. For the remainder of this report, we will refer to low solar flux and high solar flux conditions by LSF and HSF, respectively.

The data are distributed well across each bin during daytime hours and into the evening/late night hours except between 1700 and 2200 LT when the bin sizes are smaller around the PRE. There is reduced number of measurements between 0400 and 0600 LT across all seasons and solar cycles especially for altitudes above 440 km. This is due to the reduced electron densities (and increased errors) toward the end of the night, a few hours prior to sunset.

Table 1 summarizes the distribution of observation days for each season during low and high solar conditions. For reference, it also shows the average solar flux index ($F_{10.7}$ in SFU) for each season. The average solar flux is computed based on the availability of vertical and zonal plasma drift measurements.

3. Results and Discussion

We start by presenting and discussing results related to the climatology of the geomagnetically quiet vertical and zonal drifts obtained in this study. We then present and discuss results related to height variations in zonal and plasma drifts derived from the climatological estimates. Finally, we discuss the relationship between vertical and zonal drifts height profiles.

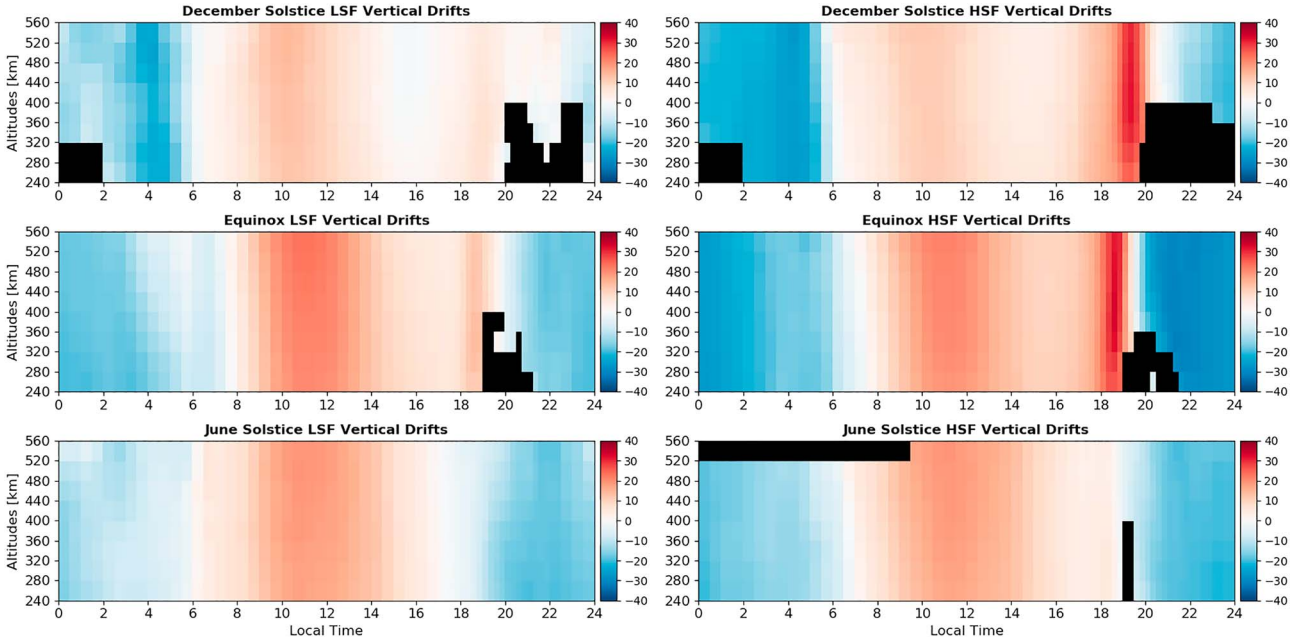

Figure 1. Variation of vertical plasma drifts as a function of local time and height for different seasons (rows) and solar flux conditions (columns). HSF = high solar flux; LSF = low solar flux.

3.1. Climatology of the Vertical Drifts

Figure 1 shows two-dimensional (2-D) color maps that summarize our results for the local time variation of the height profiles of vertical drifts for different seasons (rows) and solar flux conditions (columns).

The regions in black color indicate times and heights where either only a reduced number of measurements (less than 350 data points) were available or the variability of the drift values exceeded the typical variability of the drifts at topside heights. The reduced number of measurements and/or increased variability of the measured drifts is credited, for the most part, to the effects of reduced electron densities as well as contamination by coherent scatter echoes caused by ESF irregularities. One can notice that the regions affected are mostly in the bottomside *F* region around evening hours, where the PRE is well developed, for all seasons and solar flux conditions. The PRE raises the main *F* region to higher altitudes and creates favorable conditions for the development of postsunset ESF. We provide additional details about the causal relationship between the upward drifts and ESF later in this section.

As expected, the results in Figure 1 show that the drifts follow a diurnal pattern, being upward during the day and downward at night. The results also show the development of the PRE of the zonal electric field around sunset hours. Also following expectations, the drifts vary with season and solar flux conditions.

In order to provide a better visualization of the behavior of the estimated drift patterns, and a comparison with model expectations, we represent the results as shown in Figure 2. Figure 2 shows our average drifts (red curves) from measurements made between 300 and 400 km altitude, near the *F* region peak, where the SNR of the observed echoes and accuracy of the drift estimates are expected to be the highest. This follows the procedure used by Scherliess and Fejer (1999). The error bars represent the variability of the data points used to create the averages. The expected variation of the drifts based on the Scherliess and Fejer (1999) empirical model (SF99) is also shown (black curves) for each season and solar flux condition. The SF99 model used 502 days of ISR measurements from 1968 to 1992 at Jicamarca Radio Observatory as well as in situ satellite measurements from the Atmospheric Explorer-E satellite to expand the model to longitudes outside the Peruvian sector. Therefore, the measurements used in the SF99 and in this study can be considered virtually independent.

A comparison of our vertical drift curves with the SF99 model predictions in Figure 2 shows that our climatology of the vertical drifts reproduce very closely the seasonal and solar flux variability of the drifts predicted by the model. Perhaps more importantly, it shows that the model estimates are well within the variability (error bars) of our data sets for all local times, seasons, and solar flux conditions.

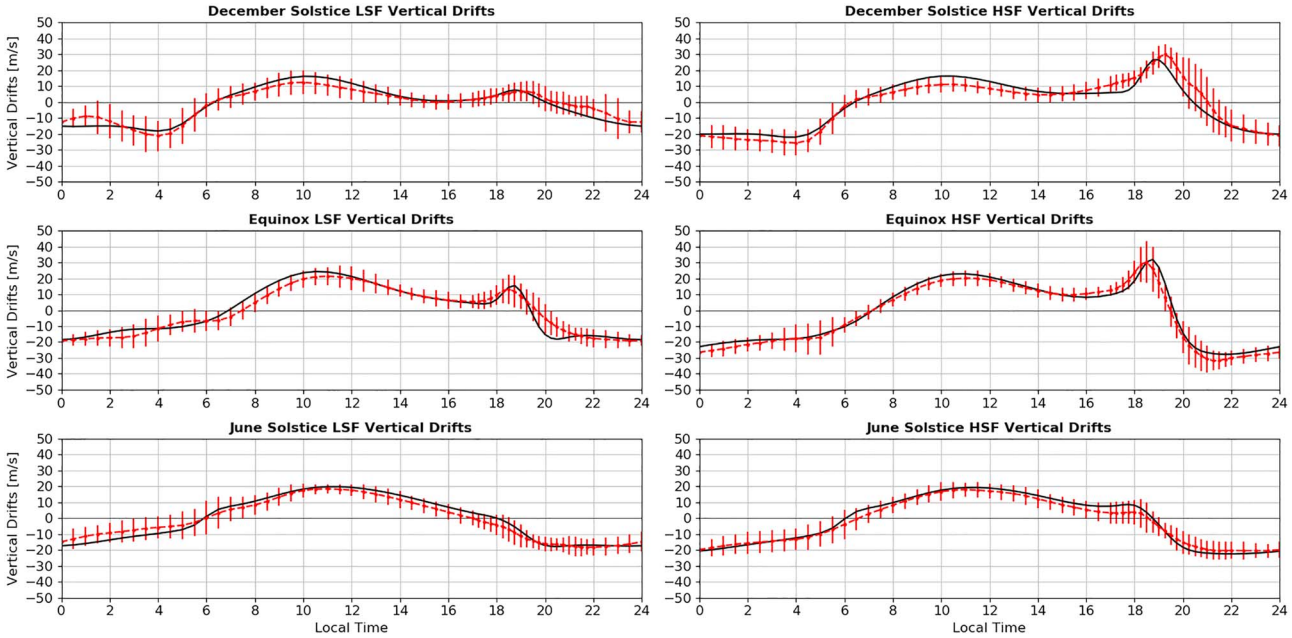

Figure 2. Variation of height-averaged (300–400 km) vertical drifts as a function of local time (red curves) for different seasons (rows) and solar flux conditions (columns). The error bars represent the variability of the drift values used to obtain the averages. The solid black curves show predictions of the Scherliess and Fejer (1999). HSF = high solar flux; LSF = low solar flux.

Figure 2 shows that daytime vertical drifts reach maximum values around 11:00 LT during June solstice and equinox. During December solstice, maximum daytime drift values occur around 10:00 LT. The maximum value of the daytime upward drifts vary with season. The largest drift peak magnitudes occur during equinox, and the weakest peaks occur during December solstice. There is little variation of the daytime drifts with solar cycle, which is consistent with the findings of Fejer et al. (1991).

We now turn our attention to the behavior of the vertical drifts during nighttime hours. The results in Figures 1 and 2 show that nighttime vertical drifts vary with season and solar flux conditions. While the pattern of the nighttime drifts change with season, the magnitude of the drifts increase with solar flux. During equinox, the downward drifts reach their peak magnitudes shortly after the PRE and slowly decreases in magnitude throughout the rest of the night before reversing the direction near sunrise. A similar pattern is seen in the June solstice drift curves. During December solstice, however, the drifts display a distinct behavior. After the PRE, the magnitude of the downward drifts increase slowly, with maximum values near 0400 LT. Finally, Figures 1 and 2 clearly show the expected development and variability of the PRE with season and solar flux. The results show that the PRE is well developed during equinox and December solstice. During June solstice, only a weak PRE is observed during the HSF.

As mentioned earlier, the behavior of the vertical drifts in the evening and nighttime hours can explain most of the morphology of ESF. The strong PRE peaks observed during equinox and December solstice explain the high occurrence of postsunset ESF in the Peruvian sector during those seasons. The weak PRE during June solstice is also in agreement with the reduced occurrence rates of ESF during the same period. Furthermore, the behavior of the drifts after the PRE peak can also explain some of the features of ESF morphology observed in the American sector. For instance, Zhan et al. (2018) recently showed, using long-term radar measurements at Jicamarca, that ESF lasted longer during December solstice than equinox. This can be explained, at least in part, by the fast transition to strong downward drifts during equinox, which creates quicker and stronger stabilizing conditions for the generalized Rayleigh-Taylor instability compared to December solstice. Finally, the observed pattern of the drift curves and their response to solar flux conditions can explain some of ESF observations during June solstice. Zhan et al. (2018) showed that noticeable occurrence rates of ESF during June solstice are limited to postmidnight hours and LSF conditions. This can be explained by the weakening of the downward drifts during LSF conditions seen in Figure 2. Combined with reduced neutral-ion collisions frequencies, and neutral winds, this can create conditions favorable for the generalized Rayleigh-Taylor instability growth. The error bars even suggest the occurrence of upward drifts

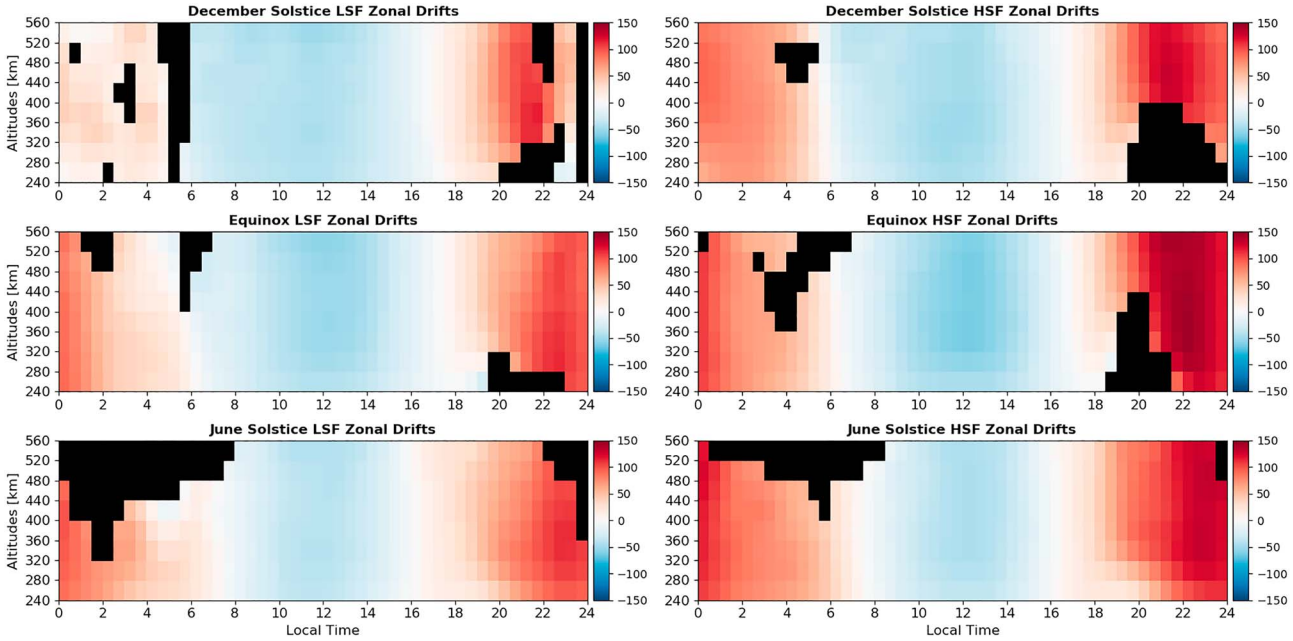

Figure 3. Variation of zonal plasma drifts as a function of local time and height for different seasons (rows) and solar flux conditions (columns). HSF = high solar flux; LSF = low solar flux.

after 0200 LT during LSF conditions. Zhan and Rodrigues (2018) have presented data-driven model analysis of the impact of weakening drifts during June solstice on postmidnight ESF observed over Jicamarca.

3.2. Climatology of the Zonal Drifts

We now present and discuss our results for the variability of zonal plasma drifts. Figure 3 shows 2-D color maps that summarize the height profiles of zonal drifts varying with local time, different seasons (rows), and solar flux conditions (columns). Again, the black bins indicate times and heights when less than 350 data points were available for analysis or when the variability of the drifts exceeded typical values for the topside region. We must point out that there were few good observations made between 0600 and 0800 LT across all seasons, particularly in the topside ionosphere. During June solstice, there was a significant lack of data at higher altitudes in the postmidnight sector.

In order to provide a better visualization of the behavior of the zonal drifts as a function of season and solar flux, we represent the results as shown in Figure 4. Each panel shows the average zonal plasma drifts between 300 and 500 km altitude for a season. The blue and red curves represent LSF and HSF conditions, respectively. We also use the curves in Figure 4 to compare our results with previous climatological findings, which were based on height-averaged drifts. For instance, previous studies of the climatology of the zonal plasma drifts using Jicamarca ISR measurements typically used average measurements between 300 and 400 km or 300 and 500 km where the drifts were assumed to be height independent (e.g., Fejer et al., 1991, 2005).

As expected, the results in Figures 3 and 4 show drifts that are westward during the day and eastward at night. The results in Figure 3 also show the development of vertical shears in the zonal plasma drifts near sunset hours. Similar to our results for the vertical drifts, we found that the daytime zonal drifts do not vary significantly with solar conditions. In general, the westward drifts reach their peak magnitude near 1200 LT and range between 40 and 60 m/s with the largest westward drifts occurring during equinox.

The average daytime zonal drifts shown in Figure 4 are in very good agreement with the average drifts presented by Fejer et al. (2005); see, for instance, their Figure 2. Our results, however, show weaker peak magnitudes in the nighttime drifts especially during HSF conditions. This is likely a result of the data sets used by Fejer et al. (2005) being binned into different conditions of solar activity. Their HSF condition curves are for a higher average solar flux index (180 SFU). Fejer et al. (2005) obtained their results using 206 days of Jicamarca ISR measurements from 1970 to 1992 and 86 days of measurements from 1994 to 2003.

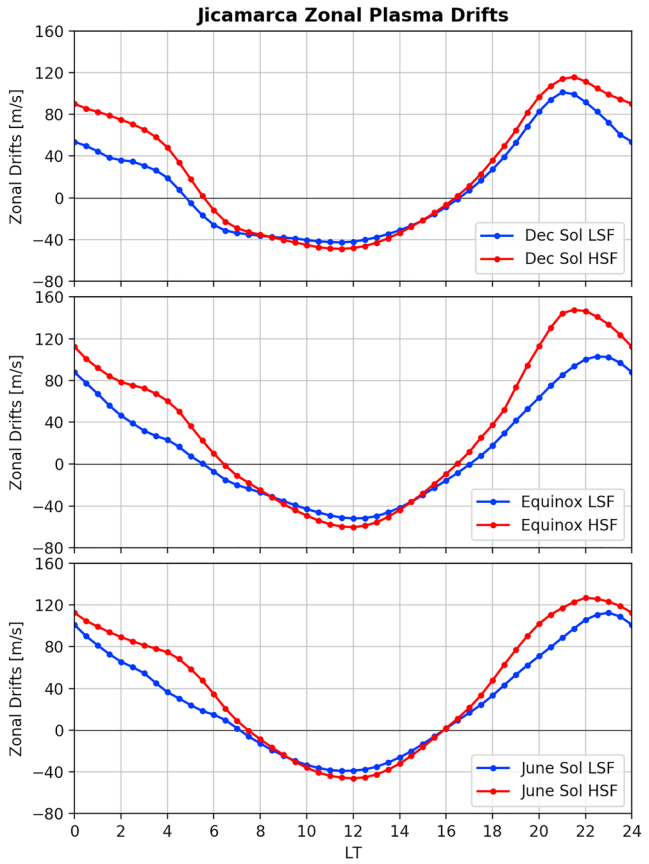

Figure 4. Variation of height-averaged (300–500 km) zonal plasma drifts as a function of local time for different seasons and solar flux conditions. HSF = high solar flux; LSF = low solar flux.

Despite data gaps, the results in Figure 3 show that beginning around 1700 LT, the zonal drifts exhibit a substantial variation with height (vertical shear) near bottomside *F* region heights. The height variation of the zonal plasma drifts is associated with the so-called evening plasma vortex, a rotational flow pattern of the plasma in the magnetic equatorial plane. The vortex has been observed in Jicamarca ISR observations for a given day (Kudeki & Bhattacharyya, 1999; Lee et al., 2015), and in average measurements of the ionospheric flow made by sensors on satellites (Eccles et al., 1999).

3.3. Height Variation of the Vertical Drifts

As mentioned earlier, previous studies indicated that height gradients in the equatorial drifts can develop. A few radar-based studies investigated this height variability. For instance, Pingree and Fejer (1987) analyzed 8 days of drift measurements made with the Jicamarca ISR during March and April (equinox) of 1986 (low solar flux conditions). They investigated the height gradients of the vertical drifts for each day. They showed that the gradients show a large day-to-day variability for nighttime hours. During daytime hours (0800–1800 LT), however, the gradients were somewhat consistent in magnitude and local time behavior. They found that the drifts varied linearly with height, having positive gradients (increasing with height) in the morning and negative gradients in the afternoon.

More recently, Rodrigues et al. (2015) compared season averages of vertical drifts estimated from 150-km echoes at Jicamarca and *F* region drift model (SF99) predictions. They also found the reoccurring pattern of increasing vertical drifts with height during morning hours and decreasing drifts in the afternoon across various conditions of solar activity. Additionally, Fejer et al. (2014) used Jicamarca ISR measurements to investigate, more closely, the height variation of the vertical drifts in the evening sector, that is, around the time when the PRE develops. They showed that the vertical drifts in that local time sector tend to increase with height below the *F* region peak and then start to decrease with height in the topside *F* region. This feature can actually be seen in our average profiles shown in Figures 5 and 6 for 1900 LT. It is more clearly observed in Figure 6, which shows results for HSF conditions. Fejer et al. (2014) pointed out that this behavior of the vertical drifts could be associated with the curl-free condition of the electric fields ($\nabla \times \mathbf{E} = 0$). We will provide further details in the following section when we return to a discussion of the zonal plasma drifts.

Figures 5 and 6 show our results for the average altitude profiles of vertical plasma drifts for LSF and HSF conditions, respectively. The profiles show that despite the small range of altitudes covered by the radar measurements, noticeable height gradients can be observed at times. In order to better quantify our results, we computed the height gradient of our average drift profiles during daytime hours when profiles have no gaps for all seasons. We determine the gradients by fitting a linear curve to the profiles for each season and solar flux condition. The results are shown in Figure 7. The top panel shows the estimated height gradient as a function of local time for each season under LSF conditions. The bottom panel shows the results for HSF conditions. Similar to Pingree and Fejer (1987), we found positive height gradients in the morning and negative gradients in the afternoon for equinox, LSF conditions. The maximum value of our gradients is also in good agreement with the values obtained by Pingree and Fejer (1987), approximately 0.01 m/s/km (that is 1 m/s per 100 km). Similar pattern is found for other seasons with the exception of June solstice HSF when gradients decrease in the afternoon but only turn negative after ~1600 LT.

Our results indicate that the gradients throughout the *F* region are modest and that vertical drifts on the topside *F* region do not differ much from the drifts at lower altitudes. We must point out, however, that gradients shown in Figure 7 are for the average height profiles of the drifts. Inspection of profiles for a given

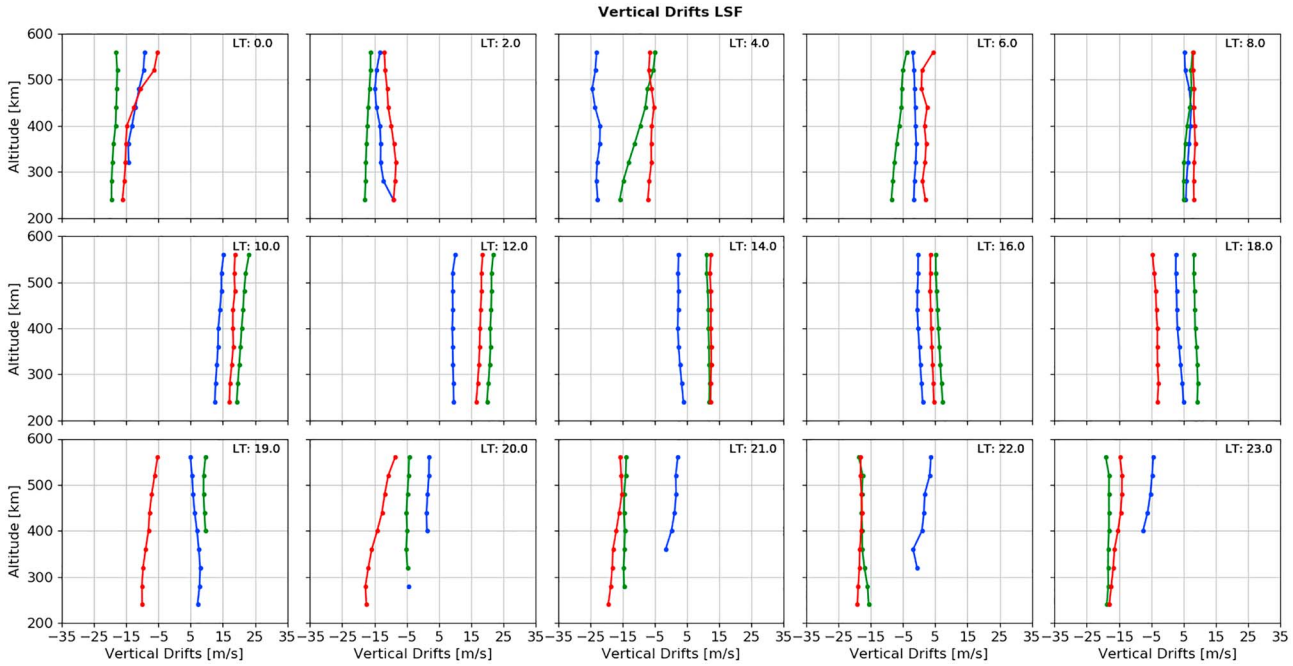

Figure 5. Height profiles of the vertical plasma drifts during low solar flux (LSF) conditions for different local times. Blue, green, and red lines represent December solstice, equinox, and June solstice, respectively.

day shows much stronger gradients. Fejer et al. (2014) shows examples of vertical drift profiles that exemplify well the large height gradients that can develop over Jicamarca, particularly in the evening sector.

3.4. Height Variation of Zonal Drifts

Figures 8 and 9 now show the height profiles of the average zonal plasma drifts for LSF and HSF conditions, respectively. The results show that during daytime, the zonal drift profiles do not vary much with height, at

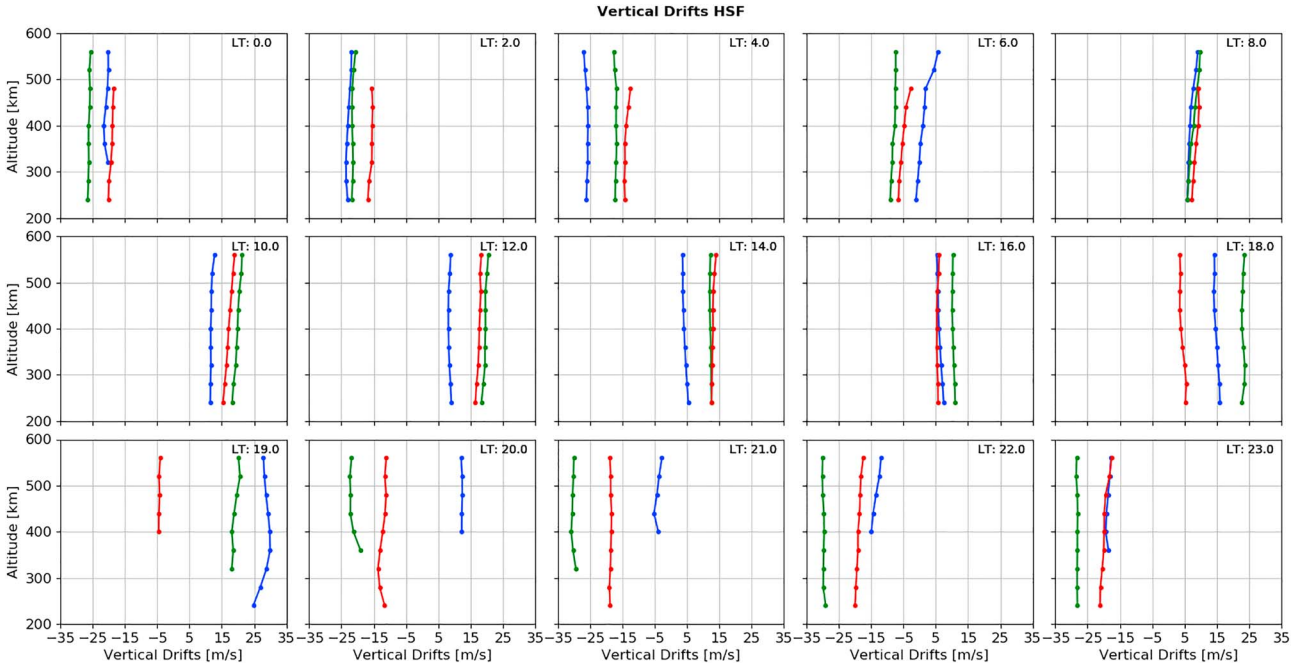

Figure 6. Height profiles of the vertical plasma drifts during high solar flux (HSF) conditions for different local times. Blue, green, and red lines represent December solstice, equinox, and June solstice, respectively.

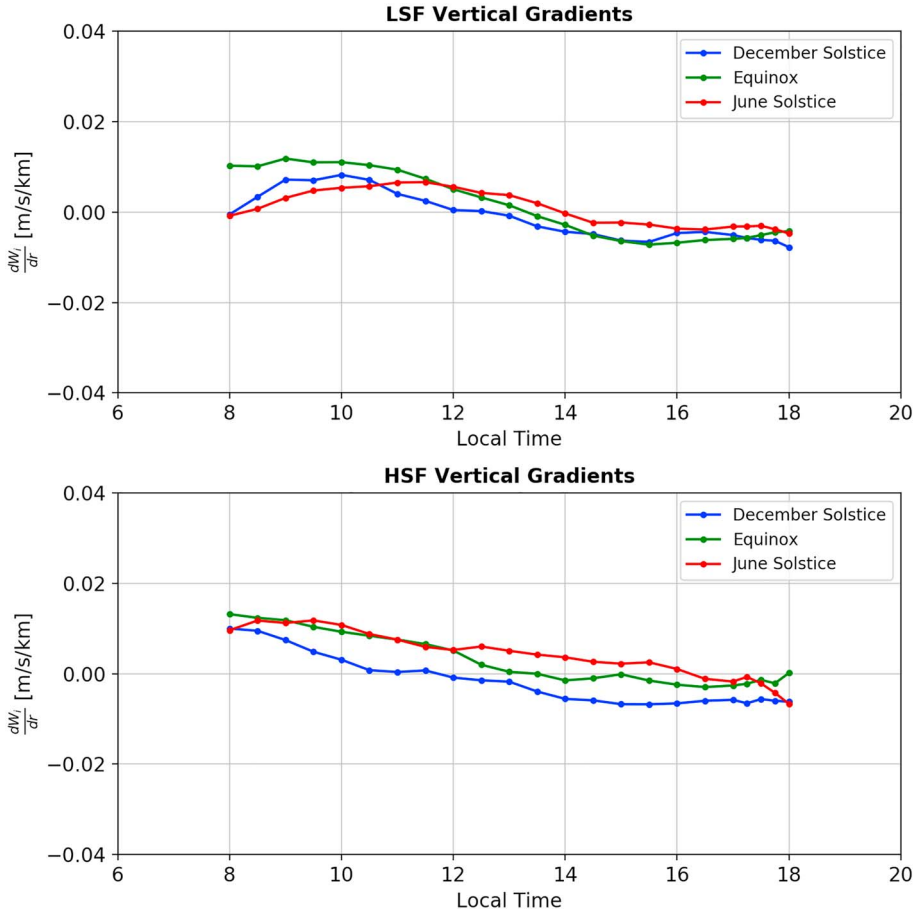

Figure 7. Local time variation of the height gradients in the averaged vertical drift profiles for LSF (top panel) and HSF (bottom panel) conditions. Blue, green, and red lines represent December solstice, equinox, and June solstice, respectively. HSF = high solar flux; LSF = low solar flux.

least throughout main F region altitudes (~200–600 km). The results also show small changes with season. Finally, comparing the results in Figures 8 and 9 also shows that the daytime profiles do not vary much with solar flux.

At night, however, the profiles for different seasons and solar flux conditions tend to diverge and vary significantly with height and time. The most striking feature of the zonal drift profiles is, perhaps, the large vertical gradient observed at lower altitudes between 1800 LT and midnight during both LSF and HSF conditions. As mentioned earlier, we associate these variations with the evening vortex pattern of the equatorial plasma drifts.

Assuming electric equipotential magnetic field lines, and a 2-D description of the low-latitude ionospheric currents, the height variation of the vertical electric field at the magnetic equator (E_v) can be described by (Haerendel et al., 1992):

$$E_v(h) = \frac{\Sigma_H(h)}{\Sigma_P(h)} E_z(h) + \frac{J_v(h)}{\Sigma_P(h)} - B(h) U_\phi^P(h), \quad (1)$$

where h represents the apex height at the magnetic equator; Σ_H and Σ_P are the field-line integrated Hall and Pedersen conductivities, respectively; E_z is the zonal component of the electric field at the magnetic equator; B is the magnetic field strength; U_ϕ^P is the field-line integrated, Pedersen conductivity weighted zonal winds; and J_v is the field-line integrated vertical current density. Rodrigues et al. (2012) used TIE-GCM simulations of the upper atmosphere, ionosphere, and electrodynamics to show that the model was able to reproduce the vortex pattern of the drifts. More importantly, they showed the contributions of each term in equation (1) to the height variation of the zonal drifts. They found that the wind-dynamo term (last term in equation (1)) was the main contributor to the height variation of the zonal drifts (shear) in the evening sector.

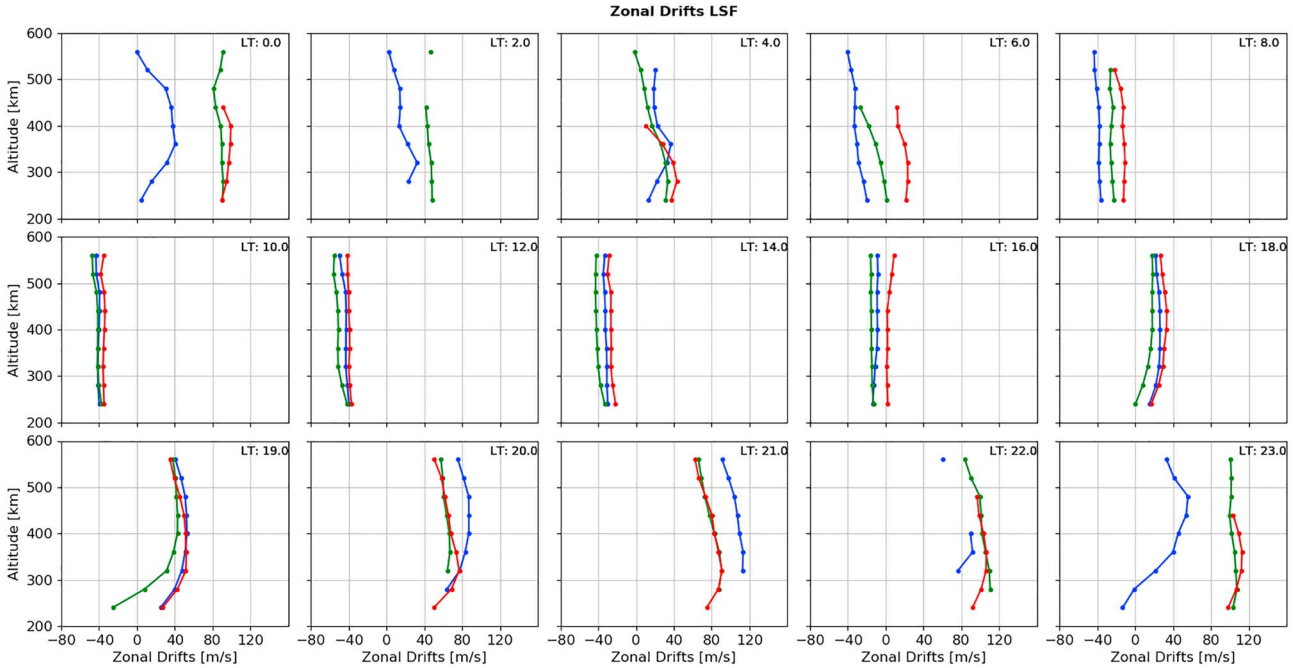

Figure 8. Height profiles of the zonal plasma drifts during low solar flux (LSF) conditions for different local times. Blue, green, and red lines represent December solstice, equinox and June solstice, respectively.

Richmond et al. (2015) conducted additional, more detailed model experiments using TIE-GCM coupled with the global ionosphere-plasmasphere model. Richmond et al. (2015) confirmed that the evening vertical shear in the equatorial zonal plasma drifts is controlled, mostly, by wind-dynamo effects and that it is strongly associated with height variations in the low-latitude thermospheric winds. Also using TIE-GCM and global ionosphere-plasmasphere simulations, Evonosky et al. (2016) further investigated the main sources of the low-latitude thermospheric wind structuring, including pressure-gradient acceleration, ion

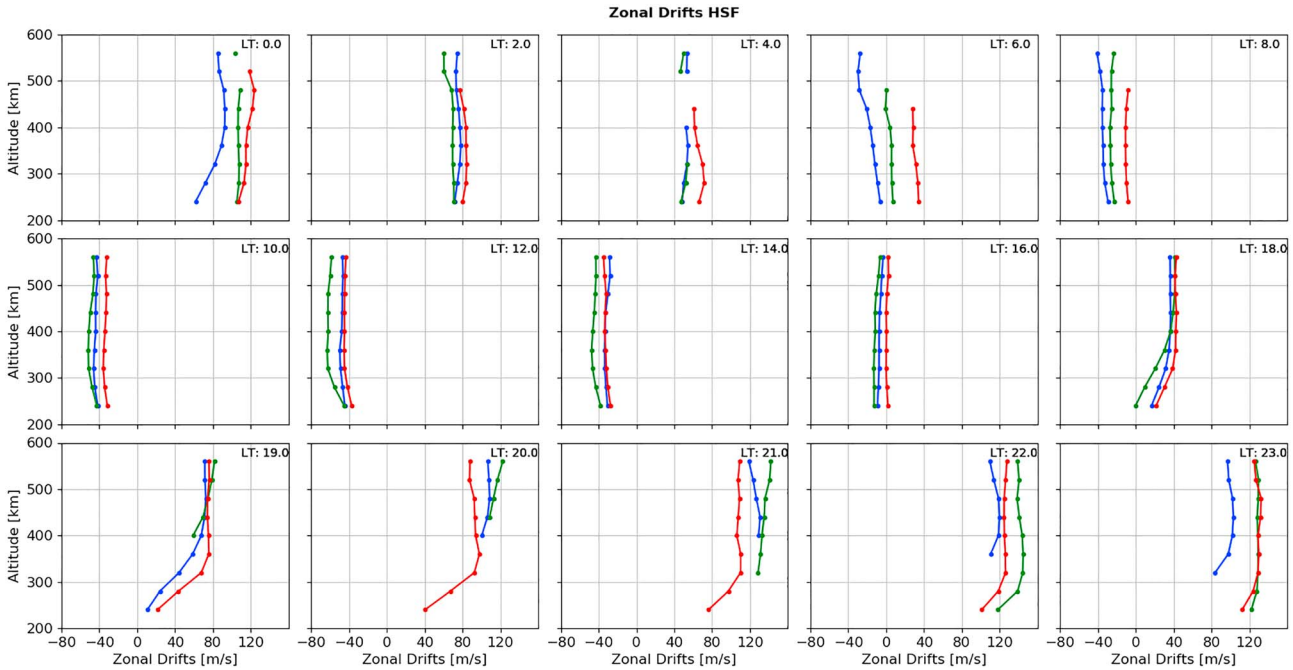

Figure 9. Height profiles of the zonal plasma drifts during high solar flux (HSF) conditions for different local times. Blue, green, and red lines represent December solstice, equinox and June solstice, respectively.

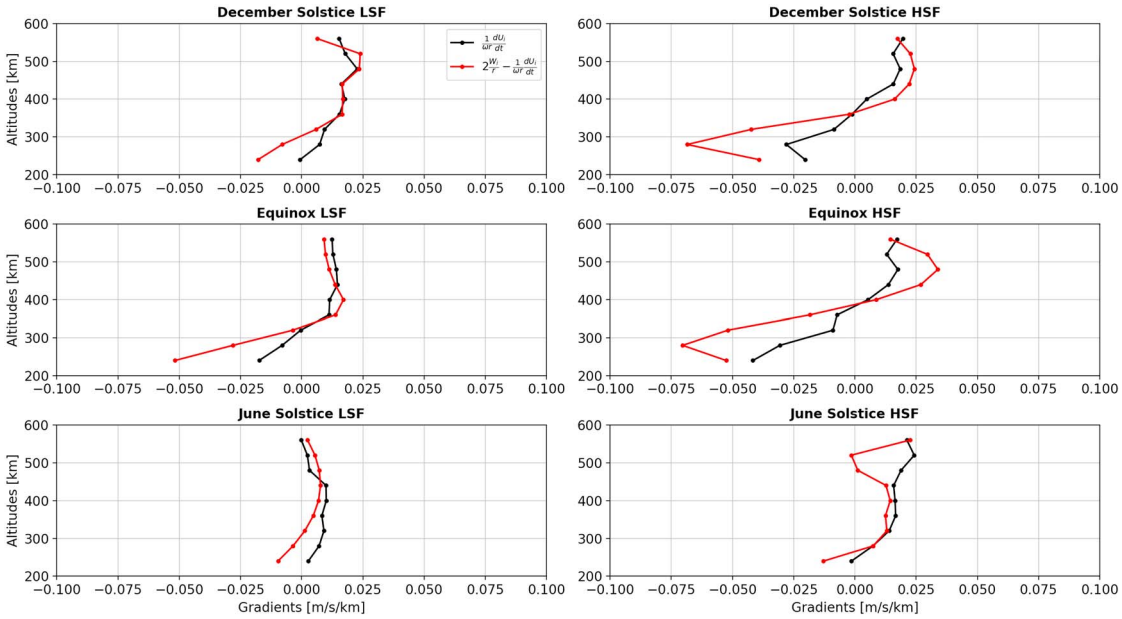

Figure 10. Height profiles of the components of $\nabla \times \mathbf{E}$ (equation (2)) estimated from our climatological estimates of the F region drifts. Results are for the time of the prereversal enhancement peak in each season. HSF = high solar flux; LSF = low solar flux.

drag, and viscous acceleration. They found that the vertical shear in the evening zonal winds is caused by a strong height variation in pressure-gradient acceleration. Strong pressure-gradient acceleration reverses the direction of daytime westward winds at high altitudes. Weak pressure-gradient acceleration at low altitudes, on the other hand, fails to create such a reversal of the zonal winds at those heights, creating a vertical shear.

Our results quantify the effects of such behavior of neutral winds in the zonal plasma drifts. The results in Figures 8 and 9 show that plasma drifts are westward and weakly dependent on height during afternoon hours (before ~1600 LT) on all seasons and solar flux conditions. By 1800 LT zonal drifts at upper altitudes (above ~300 km) have already been strongly accelerated in the eastward direction. Zonal plasma drifts at lower altitudes, however, accelerate more slowly due to, supposedly, weaker wind velocities at those heights. A vertical gradient in the zonal drifts starts to develop. By 1900 LT the evening vertical shear in the zonal plasma drifts can be seen in all seasons. Lastly, model results of Richmond et al. (2015) indicated a lack of positive correlation between the PRE and the shear in the zonal drifts. Our results indeed show that only a weak PRE occurs despite a somewhat strong shear in the zonal plasma drifts for June solstice HSF.

3.5. Relationship Between Vertical and Zonal Drifts

Finally, in order to further test the accuracy of our climatological estimates of the drift profiles and better understand their variability, we now evaluate the consistency between zonal and vertical drifts. This evaluation follows the electrostatic analysis proposed by Murphy and Heelis (1986). At the magnetic equator, assuming a static dipole magnetic field, the curl-free condition for ionopsheric F region electric fields, that is, $\nabla \times \mathbf{E} = \nabla \times (-\mathbf{v} \times \mathbf{B}) = 0$, leads to the following relationship (Murphy & Heelis, 1986):

$$\frac{1}{r}\frac{\partial U_i}{\partial \phi} = \frac{2W_i}{r} - \frac{\partial W_i}{\partial r}, \tag{2}$$

where W_i and U_i are the components of the equatorial $\mathbf{E} \times \mathbf{B}F$ region plasma drifts in the radial (r) and zonal/longitudinal (ϕ) directions, respectively. Assuming that time and longitudinal variations of zonal drifts are interchangeable, equation (2) shows that height variations in the vertical drifts should be followed by correspond to longitudinal variations in the zonal drifts. Pingree and Fejer (1987) used height-averaged drift measurements at Jicamarca to find results that supported the curl-free condition (equation (2)) for the ionospheric electric fields. We now use equation (2) to test the accuracy and self-consistency of our estimates of zonal and vertical drifts as a function of height. For this test, we select the period of the PRE when the height variation of the vertical drifts and the longitudinal variation of the zonal drifts are expected to exceed, or at least be comparable to, the variability of the drifts used to generate the averages.

Figure 10 shows the height variation of the terms in equation (2) for the time of the PRE peak for all seasons and solar flux conditions. The black curves represent the left-hand side of equation (2), which depends only on the longitudinal gradients in the zonal drifts. The red curves, on the other hand, represent the right hand side of equation (2), and depends only on the height variation of the vertical drifts. The derivatives were computed using a third-order B-spline fit to the drifts. The agreement between both estimates is very good for all seasons and solar flux conditions, despite the fact that each drift profile is formed by averaging a wide range of days and solar flux conditions. It is also expected that small scale (tens to few hundreds of km) variations in winds and/or conductivity produce zonal variations in the electric fields. These variations would violate, at times, our assumption of interchangeability between local time and longitude.

Nevertheless, the results suggest that one could obtain a first-order estimate of the longitudinal (or local time) variation of the zonal drifts from the height variation of vertical drifts at least during the PRE time. More importantly, the results indicate a good agreement between our climatologies of the zonal and vertical drifts.

4. Conclusions

We presented and discussed the results of an analysis of long-term measurements of geomagnetically quiet ionospheric *F* region $\mathbf{E} \times \mathbf{B}$ plasma drifts in the American/Peruvian sector. The analysis used observations made between 1986 and 2017 by the ISR of the Jicamarca Radio Observatory. Unlike previous studies, we analyzed both vertical and zonal components of the plasma drifts to derive the climatological variation of the drifts as a function of *F* region heights (240–560 km) and local time. We were able to determine the average behavior of the height profiles of the drifts for different seasons and distinct (low and high) solar flux conditions. Of particular importance is the fact that the mean solar flux conditions for both vertical and zonal plasma drift climatologies were the same. This allows our results to be used in evaluating both components of the transverse (to **B**) electric fields predicted by physics-based models, for instance.

Our results show overall good agreement with previous height-averaged climatologies of vertical and zonal plasma drifts, despite results being obtained from different sets of measurements. More importantly, our results quantify height variations in the drifts. Our results show that the height gradients of our average daytime vertical drift profiles are typically small (1 m/s every 100 km). We must point out that inspection of drift profiles for a given day, however, shows much stronger height gradients. This is important for studies such as those trying to correlate vertical drifts measured at LEO satellite altitudes and ESF (e.g., Huang & Hairston, 2015; Smith et al., 2015). It is possible that the drifts measured by satellites at field lines with apex heights in the topside equatorial *F* region can vary drastically from the drifts at bottomside *F* region altitudes. Our results also show the effects of solar flux over the height variation of the vertical drifts. Stronger negative height gradients are observed in the afternoon sector at low solar flux than during high solar flux conditions.

Our results also quantify the morphology the zonal drift profiles. We show that daytime zonal drifts do not vary much with height at main *F* region altitudes. The daytime zonal drift profiles also do not vary much with season and solar flux conditions. Nighttime zonal drift profiles, on the other hand, show significant variations with height, season, and solar activity. The vertical shear in the zonal drifts associated with the evening plasma vortex is quantified for different geophysical conditions. Our results can be used to drive (or guide) models that evaluate the stability of the equatorial ionosphere and the impact of the vertical shear in the zonal drifts on ESF (e.g., Aveiro & Hysell, 2010; Hysell & Kudeki, 2004; Kudeki et al., 2007). Comparison of our results with physics-based models of the ionospheric electrodynamics can help identify the relative contribution of different sources (equation (1)) of vertical polarization electric fields.

Finally, we evaluated the agreement between our results for the vertical and zonal drift profiles using the assumption of curl-free electric fields and interchangeability between longitude and local time. We found good consistency between our zonal and vertical drifts, despite the large variability of the drifts used in our averages, and the assumption that local time and longitude are interchangeable.

Acknowledgments
The radar measurements used in this study can be obtained from the Madrigal database (http://jro.igp.gob.pe/madrigal/). The Jicamarca Radio Observatory is a facility of the Instituto Geofisico del Peru operated with support from the NSF (AGS-1433968) through Cornell University. Work at UT Dallas was supported by the NSF (AGS-1554926) and by NASA (80NSSC18K1203).

References

Aveiro, H. C., & Hysell, D. L. (2010). Three-dimensional numerical simulation of equatorial F region plasma irregularities with bottomside shear flow. *Journal of Geophysical Research*, *115*, A11321. https://doi.org/10.1029/2010JA015602

Balan, N., & Bailey, G. J. (1995). Equatorial plasma fountain and its effects: Possibility of an additional layer. *Journal of Geophysical Research*, *100*(A11), 21,421–21,432. https://doi.org/10.1029/95JA01555

Baron, M. (2013). *Probability and statistics for computer scientists*. Boca Raton, FL: CRC Press.
Chau, J. L., Fejer, B. G., & Goncharenko, L. P. (2009). Quite variability of equatorial ExB drifts during a sudden stratospheric warming event. *Geophysical Research Letters*, *36*, L05101. https://doi.org/10.1029/2008GL036785
Chau, J., Fejer, B. G., Goncharenko, L. P., & Liu, H.-L. (2012). Equatorial and low latitude ionospheric effects during sudden stratospheric warming events. *Space Science Reviews*, *168*, 385–417. https://doi.org/10.1007/s11214-011-9797-5
Coley, W. R., Heelis, R. A., & Spencer, N. W. (1994). Comparison of low-latitude ion and neutral zonal drifts using DE 2 data. *Journal of Geophysical Research*, *99*(A1), 341–348. https://doi.org/10.1029/93JA02205
Eccles, J. V. (2004). The effect of gravity and pressure in the electrodynamics of the low-latitude ionosphere. *Journal of Geophysical Research*, *109*, A05304. https://doi.org/10.1029/2003JA010023
Eccles, J. V., Maynard, N., & Wilson, G. (1999). Study of the evening plasma drift vortex in the low-latitude ionosphere using San Marco electric field measurements. *Journal of Geophysical Research*, *104*(A12), 28,133–28,143. https://doi.org/10.1029/1999JA900373
Evonosky, W., Richmond, A. D., Fang, T.-W., & Maute, A. (2016). Ion-neutral coupling effects on low-latitude thermospheric evening winds. *Journal of Geophysical Research: Space Physics*, *121*, 4638–4646. https://doi.org/10.1002/2016JA022382
Fejer, B. G., de Paula, E. R., Gonzalez, S. A., & Woodman, R. F. (1991). Average vertical and zonal F region plasma drifts over Jicamarca. *Journal of Geophysical Research*, *96*(A8), 13,901–13,906. https://doi.org/10.1029/91JA01171
Fejer, B. G., Farley, D. T., Gonzales, C. A., Woodman, R. F., & Calderon, C. (1981). F region east-west drifts at Jicamarca. *Journal of Geophysical Research*, *86*(A1), 215–218. https://doi.org/10.1029/JA086iA01p00215
Fejer, B., Farley, D., Woodman, R., & Calderon, C. (1979). Dependence of equatorial F region vertical drifts on season and solar cycle. *Journal of Geophysical Research*, *84*(A10), 5792–5796. https://doi.org/10.1029/JA084iA10p05792
Fejer, B. G., Hui, D., Chau, J. L., & Kudeki, E. (2014). Altitudinal dependence of evening equatorial F region vertical plasma drifts. *Journal of Geophysical Research: Space Physics*, *119*, 5877–5890. https://doi.org/10.1002/2014JA019949
Fejer, B. G., Jensen, J. W., & Shin-Yi, Su (2008). Quiet time equatorial F region vertical plasma drift model derived from ROCSAT-1 observations. *Journal of Geophysical Research*, *113*, A05304. https://doi.org/10.1029/2007JA012801
Fejer, B. G., Kudeki, E., & Farley, D. T. (1985). Equatorial F region zonal plasma drifts. *Journal of Geophysical Research*, *90*(A12), 12,249–12,255. https://doi.org/10.1029/JA090iA12p12249
Fejer, B. G., Santos, A. S., & Costa Pereira, A. E. (2005). Climatology of F region zonal plasma drifts over Jicamarca. *Journal of Geophysical Research*, *110*, A12310. https://doi.org/10.1029/2005JA011324
Fejer, B. G., & Scherliess, L. (1995). Time-dependent response of equatorial ionospheric electric fields to magnetospheric disturbances. *Geophysical Research Letters*, *22*, 85–854. https://doi.org/10.1029/95GL00390
Fejer, B. G., Scherliess, L., & dePaula, E. R. (1999). Effects of the vertical plasma drift velocity on the generation and evolution of equatorial spread F. *Journal of Geophysical Research*, *104*(A9), 19,859–19,869. https://doi.org/10.1029/1999JA900271
Haerendel, G., Eccles, J. V., & ÄĞakir, S. (1992). Theory for modeling the equatorial evening ionosphere and the origin of the shear in the horizontal plasma flow. *Journal of Geophysical Research*, *97*(A2), 1209–1223. https://doi.org/10.1029/91JA02226
Herrero, F. A., Mayr, H. G., Spencer, N. W., Hedin, A. E., & Fejer, B. G. (1985). Interaction of zonal winds with the magnetic pressure bulge in the Earth's thermosphere: Empirical check of momentum balance. *Geophysical Research Letters*, *12*, 491–494. https://doi.org/10.1029/GL012i008p00491
Huang, C., & Hairston, M. R. (2015). The postsunset vertical plasma drift and its effects on the generation of equatorial plasma bubbles observed by the C/NOFS satellite. *Journal of Geophysical Research: Space Physics*, *120*, 2263–2275. https://doi.org/10.1002/2014JA020735
Hysell, D. L. (2000). An overview and synthesis of plasma irregularities in equatorial spread F. *Journal of Atmospheric and Solar-Terrestrial Physics*, *62*(12), 1037–1056. https://doi.org/10.1016/S1364-6826(00)00095-X
Hysell, D. L., & Kudeki, E. (2004). Collisional shear instability in the equatorial F region ionosphere. *Journal of Geophysical Research*, *109*, A11301. https://doi.org/10.1029/2004JA010636
Kil, H., Oh, S.-J., Paxton, L. J., & Fang, T.-W. (2009b). High-resolution vertical ExB drift model derived from ROCSAT-1 data. *Journal of Geophysical Research*, *114*, A10314. https://doi.org/10.1029/2009JA014324
Kil, H., Paxton, L. J., & Oh, S.-J. (2009a). Global bubble distribution seen from ROCSAT-1 and its association with the evening prereversal enhancement. *Journal of Geophysical Research*, *114*, A06307. https://doi.org/10.1029/2008JA013672
Kudeki, E., & Bhattacharyya, S. (1999). Postsunset vortex in equatorial F-region plasma drifts and implications for bottomside spread-F. *Journal of Geophysical Research*, *104*(A12), 28,163–28,170. https://doi.org/10.1029/1998JA900111
Kudeki, E., Bhattacharyya, S., & Woodman, R. F. (1999). A new approach in incoherent scatter F region ExB drift measurements at Jicamarca. *Journal of Geophysical Research*, *104*(A12), 28,145–28,162. https://doi.org/10.1029/1998JA900110
Kudeki, E., Akgiray, A., Milla, M., Chau, J. L., & Hysell, D. L. (2007). Equatorial spread-F initiation: Post-sunset vortex, thermospheric winds, gravity waves. *Journal of Atmospheric and Solar-Terrestrial Physics*, *69*, 2416–2427. https://doi.org/10.1016/j.jastp.2007.04.012
Lee, W. K., Kil, H., Kwak, Y.-S., & Paxton, L. J. (2015). Morphology of the postsunset vortex in the equatorial ionospheric plasma drift. *Geophysical Research Letters*, *42*, 9–14. https://doi.org/10.1002/2014GL062019
Murphy, J. A., & Heelis, R. (1986). Implications of the relationship between electromagnetic drift components at mid and low latitudes. *Planetary and Space Science*, *34*, 645–652. https://doi.org/10.1016/0032-0633(86)90042-5
Pingree, J. E., & Fejer, B. G. (1987). On the height variation of equatorial F region vertical plasma drifts. *Journal of Geophysical Research*, *92*(A5), 4763–4766. https://doi.org/10.1029/JA092iA05p04763
Richmond, A. D., Fang, & Maute, A. (2015). Electrodynamics of the equatorial evening ionosphere: 1. Importance of winds in different regions. *Journal of Geophysical Research: Space Physics*, *120*, 2118–2132. https://doi.org/10.1002/2014JA020934
Rodrigues, F. S., Crowley, G., Heelis, R. A., Maute, A., & Reynolds, A. (2012). On TIE-GCM simulation of the evening equatorial plasma vortex. *Journal of Geophysical Research*, *117*, A05307. https://doi.org/10.1029/2011JA017369
Rodrigues, F. S., Smith, J. M., Milla, M., & Stoneback, R. A. (2015). Daytime ionospheric equatorial vertical drifts during the 2008-2009 extreme solar minimum. *Journal of Geophysical Research: Space Physics*, *120*, 1452–1459. https://doi.org/10.1002/2014JA020478
Scherliess, L., & Fejer, B. G. (1999). Radar and satellite global equatorial F region vertical drift model. *Journal of Geophysical Research*, *104*, 6829–6842. https://doi.org/10.1029/1999JA900025
Stoneback, R. A., Heelis, R. A., Burrell, A. G., Coley, W. R., Fejer, B. G., & Pacheco, E. (2011). Observations of quiet time vertical ion drift in the equatorial ionosphere during the solar minimum period of 2009. *Journal of Geophysical Research*, *116*, A12327. https://doi.org/10.1029/2011JA016712
Smith, J. M., Rodrigues, F. S., & de Paula, E. R. (2015). Radar and satellite investigations of equatorial evening vertical drifts and spread F. *Annales Geophysicae*, *33*, 1403–1412. https://doi.org/10.5194/angeo-33-1403-2015
Woodman, R. F. (1972). East-west ionospheric drifts at the magnetic equator. In *Space research XII; Proceedings of the Fourteenth Plenary Meeting, Seattle, Wash., June 18-July 2, 1971. Volume 2. Berlin, East Germany, Akademie-Verlag GmbH* (pp. 969–974).

Zhan, W., & Rodrigues, F. S. (2018). June solstice equatorial spread F in the American sector: A numerical assessment of linear stability aided by incoherent scatter radar measurements. *Journal of Geophysical Research: Space Physics*, *123*, 755–767. https://doi.org/10.1002/2017JA024969

Zhan, W., Rodrigues, F. S., & Milla, M. A. (2018). On the genesis of postmidnight equatorial spread F: Results for the American/Peruvian sector. *Geophysical Research Letters*, *45*, 7354–7361. https://doi.org/10.1029/2018GL078822

Woodman, R. F (2009). Spread F—An old equatorial aeronomy problem finally resolved? *Annals of Geophysics*, *27*, 1915–1934. https://doi.org/10.5194/angeo-27-1915-2009